JHEP|Reports

The efficacy of atezolizumab plus bevacizumab for advanced hepatocellular carcinoma in relation to tumor-infiltrating lymphocytes

Authors

Hiroaki Kanzaki, Takamasa Ishino, Sadahisa Ogasawara, …, Yujin Hoshida, Mina Komuta, Yosuke Togashi

Correspondence

ogasawaras@chiba-u.jp (S. Ogasawara).

Graphical abstract

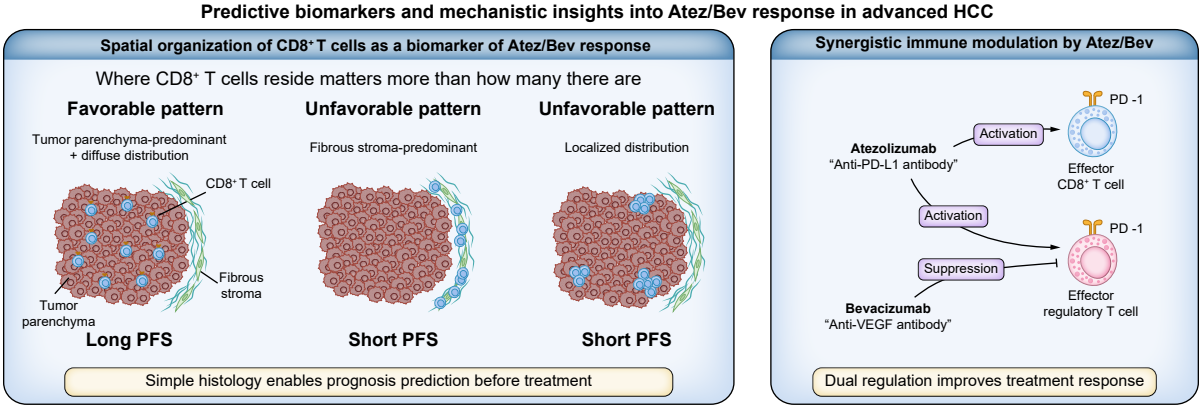

Highlights:

- High PD-1 positivity in CD8$^+$ T cells predicts favorable outcomes in patients treated with atezolizumab and bevacizumab.
- Tumor parenchyma-predominant localization and diffuse distribution of CD8$^+$ T cells predict improved treatment response.
- These spatial features can be assessed from pretreatment biopsies using routine H&E staining and CD8 immunohistochemistry.
- Bevacizumab suppresses effector regulatory T-cell activation, mitigating the potential adverse effect of PD-L1 blockade.

Impact and implications:

This study demonstrates that the localization and distribution pattern of CD8$^+$ T cells within the tumor parenchyma are predictors of atezolizumab plus bevacizumab treatment outcomes in advanced hepatocellular carcinoma. The study further reveals that bevacizumab counteracts the potentially unfavorable influence of programmed death-ligand 1 blockade by suppressing effector regulatory T-cell activation. These findings provide both a valuable guide for determining treatment strategies in routine clinical practice and a foundation for future immunotherapy development for the treatment of advanced hepatocellular carcinoma.

https://doi.org/10.1016/j.jhepr.2025.101614

Research article

JHEP|Reports

The efficacy of atezolizumab plus bevacizumab for advanced hepatocellular carcinoma in relation to tumor-infiltrating lymphocytes

Hiroaki Kanzaki[1,2,†], **Takamasa Ishino**[1,3,†], **Sadahisa Ogasawara**[1,*,†], Takahiro Tsuchiya[1], Makoto Fujiya[1], Midori Sawada[1], Ryo Izai[1], Teppei Akatsuka[1], Chihiro Miwa[1], Takuya Yonemoto[1], Sae Yumita[1], Miyuki Nakagawa[1], Ryuta Kojima[1], Keisuke Koroki[1], Masanori Inoue[1], Kazufumi Kobayashi[1], Naoya Kanogawa[1], Masato Nakamura[1], Takayuki Kondo[1], Shingo Nakamoto[1], Tsukasa Takayashiki[4], Yuka Takano[3], Kaho Takata[3], Jason Lin[5], Masahito Kawazu[5], Jun-ichiro Ikeda[6], Masayuki Ohtsuka[4], Yujin Hoshida[2], Mina Komuta[1,7], Yosuke Togashi[1,3,8,9]

JHEP Reports **2025**. vol. 7 | 1–13

Background & Aims: Atezolizumab plus bevacizumab (Atez/Bev) improves prognosis in advanced hepatocellular carcinoma, but its mechanisms remain unclear. This study aims to identify predictive biomarkers through a comprehensive analysis of the tumor microenvironment.

Methods: Biopsy samples from 94 patients with advanced hepatocellular carcinoma before Atez/Bev were analyzed using immunohistochemistry, bulk RNA-sequencing, flow cytometry, and multiplexed imaging. The tumor microenvironment assessment included profiling of $CD8^+$ T cells and effector regulatory T (eTreg) cells. Immune dynamics were examined across baseline, in-treatment, and progression samples from each patient.

Results: We found favorable progression-free survival to be associated with a high percentage of programmed death-1 (PD-1) positivity in $CD8^+$ T cells but not with $CD8^+$ T-cell density. PD-1 positivity in $CD8^+$ T cells was dichotomized at the median (58%). Building upon PD-1 positivity in $CD8^+$ T cells, predominant and diffuse infiltration of $CD8^+$ T cells within the tumor parenchyma was shown to be associated with improved treatment response. PD-1 positivity in eTreg cells was not associated with prognosis. Finally, we found that Bev, an antivascular endothelial growth factor antibody, suppresses the eTreg-cell activation induced by programmed death-ligand 1 (PD-L1) blockade.

Conclusions: We demonstrate that immunohistochemistry analysis to determine the localization and distribution of $CD8^+$ T cells within the tumor is a viable means of predicting treatment efficacy for Atez/Bev and provides a valuable framework for future trial design. This is an exploratory analysis with no current consequences in clinical practice. Future studies should confirm the results in an external cohort.

Clinical trials registration: The study protocol was registered on the University Hospital Medical Information Network Clinical Trials Registry (UMIN-CTR) (UMIN000047701).

Introduction

Hepatocellular carcinoma (HCC), the predominant form of primary liver cancer, is the second most lethal cancer worldwide with rapidly increasing incidence rates.[1–4] Because of late diagnosis and high recurrence rates, effective systemic treatment is critical to address this significant public health challenge.[4] The introduction of atezolizumab and bevacizumab (Atez/Bev) combination therapy marked a paradigm shift in the treatment of advanced HCC, establishing a novel immunotherapeutic standard of care.[5,6] Although Atez/Bev has demonstrated remarkable efficacy in advanced HCC, the molecular determinants of treatment response remain incompletely understood, highlighting the urgent need for predictive biomarkers to enable precision medicine approaches.

The tumor microenvironment (TME), a complex ecosystem of cancer cells that interact with immune cells and fibroblasts, represents a promising source of predictive biomarkers.[7] Studies of the TME in HCC have identified potential immunotherapy-associated biomarkers and molecular subtypes.[8,9] Analysis of samples from clinical trials has shown that patients with pre-existing immunity, characterized by effector T-cell signatures and $CD8^+$ T-cell density, demonstrate better responses to Atez/Bev.[10] While these findings suggest

* Corresponding author. Address: Department of Gastroenterology, Graduate School of Medicine, Chiba University, 1-8-1 Inohana, Chuo-ku, Chiba, Japan. Tel.: +81 43 226 2083; fax: +81 43 226 2088.
E-mail address: ogasawaras@chiba-u.jp (S. Ogasawara).
† These authors contributed equally to this work.
https://doi.org/10.1016/j.jhepr.2025.101614

potential predictive factors, translation into clinically applicable biomarkers for combination immunotherapy in advanced HCC remains challenging. Most studies utilize archived samples from initial diagnosis when combination immunotherapy is not yet indicated; however, the TME may evolve significantly by the time disease progresses to require combination immunotherapy.[11] To overcome the challenges of obtaining samples from patients with advanced HCC, we previously established a safe tumor sampling protocol,[12] which we utilized to collect samples immediately before Atez/Bev initiation.

Atez blocks programmed death-1 (PD-1)/programmed death-ligand 1 (PD-L1) signaling to reinvigorate effector CD8$^+$ T cells, while Bev normalizes tumor vessels and potentially modulates effector regulatory T (eTreg) cells.[10,13] In several cancer types, PD-1/PD-L1 blockade has been shown to activate both effector CD8$^+$ T cells and eTreg cells, potentially limiting therapeutic efficacy.[14,15] However, whether these immune dynamics similarly occur in HCC, especially in the context of combination therapy with Atez/Bev, remains unknown. In this study, we investigated the potential of effector CD8$^+$ T cells and eTreg cells as predictive biomarkers of response to Atez/Bev in advanced HCC. Furthermore, we sought to associate these immune features with pathological characteristics to identify candidate biomarkers that could be evaluated using routine clinical samples.

Patients and methods

This retrospective study included two independent patient cohorts. The derivation cohort consisted of patients who received Atez/Bev between October 2020 and December 2022 at Chiba University Hospital. The validation cohort consisted of patients treated between January 2023 and December 2024 at the same institution. Tumor biopsies were performed immediately before the initiation of Atez/Bev treatment. Comprehensive analysis of tumor samples from patients with advanced HCC was performed using immunohistochemistry (IHC), bulk RNA-sequencing, flow cytometry, and multiplexed imaging. Detailed methods are provided in the Supplementary Materials.

Results

Molecular and immunological features

We collected biopsy samples according to our protocol from 94 patients with advanced HCC who received Atez/Bev in the derivation cohort (details regarding clinical characteristics and treatment outcomes are provided in the Supplementary Results). Of these patients, we obtained tumor samples suitable for pathological evaluation from 81, confirming the HCC diagnosis (Table S1). Among these patients, CD8 IHC staining was successfully performed in 77 cases. Bulk RNA-sequencing yielded analyzable data in 63 cases. Flow cytometry provided interpretable results for CD8$^+$ T cells in 53 cases and for eTreg cells in 44 cases. Multiplexed imaging was performed in 13 cases (Fig. S1). Variations in sample numbers reflect the limited biopsy material available and its stepwise allocation across platforms, as well as the exclusion of samples with insufficient data quality for reliable interpretation.

We evaluated molecular and immunological features using previously reported subclasses, signatures, and related genes (Fig. 1A).[10,16–23] Immune classification revealed a distribution of inflamed and non-inflamed classes that paralleled previous reports,[17,24] despite analyzing advanced-stage disease.

Upon analyzing the relationships between the molecular and immunological features, we found that the inflamed signature was strongly correlated with CD8$^+$ T-cell density and the enrichment of previously reported immune-related signatures (Fig. 1B). However, neither the percentage of PD-1 positivity in CD8$^+$ T cells nor eTreg cells showed a significant correlation with the inflamed signature. No further correlations were found between these immunological parameters (PD-1 positivity in CD8$^+$ T cells and eTreg cells) and the various clinical characteristics (Fig. 1B). Additionally, we further focused on serum alpha-fetoprotein (AFP) levels and compared patients with high AFP levels (>400 ng/ml) and those with low AFP levels (≤400 ng/ml) in terms of PD-1 positivity in CD8$^+$ T cells, PD-1 positivity in eTreg cells, and CD8$^+$ T-cell density. No significant differences were observed between the two groups, and these results are presented in Fig. S2.

Associations between the treatment efficacy and immunological features

Kaplan–Meier plots and hazard ratios (HRs) of progression-free survival (PFS) for the percentage of PD-1 positivity in CD8$^+$ T cells and eTreg cells, and CD8$^+$ T-cell density are shown in Fig. 2A. Fig. 2B presents a comparison of PD-1 positivity in CD8$^+$ T cells and eTreg cells, as well as CD8$^+$ T-cell density, between patients with and without disease control, while Fig. 2C illustrates the same variables stratified by clinical benefit status.

We found that high PD-1 positivity in CD8$^+$ T cells was significantly associated with favorable PFS (HR, 0.24; 95% CI, 0.11–0.52; log-rank: p <0.001). This association remained significant after adjustment for potential prognostic clinical variables, supporting the role of PD-1 positivity in CD8$^+$ T cells as an independent predictor (Table S2). Moreover, PD-1 positivity in CD8$^+$ T cells was significantly higher in both disease control (p = 0.049) and clinical benefit groups (p = 0.003), further supporting its predictive relevance. In contrast, PD-1 positivity in eTreg cells showed no significant association with either PFS (HR, 0.75; 95% CI, 0.34–1.62; log-rank: p = 0.561) or treatment response (non-disease control: p = 0.860; non-clinical benefit: p = 0.618). Notably, neither CD8$^+$ T-cell density (HR, 1.12; 95% CI, 0.64–1.95; log-rank: p = 0.156; disease control: p = 0.999; clinical benefit: p = 0.586) nor previously reported immune-related signatures showed significant associations with clinical outcomes (Fig. 2D).[10,17–23] To further explore immune-related features associated with clinical outcome, we also evaluated the presence of tertiary lymphoid structures (TLS) or immune aggregates within the tumor parenchyma. In this cohort, the presence of even a single TLS or immune aggregate was not associated with favorable PFS (HR, 0.73; 95% CI, 0.29–1.86; log-rank p = 0.511) (Fig. S3A).

To address potential concerns regarding assay-specific patient heterogeneity, we additionally conducted a subgroup analysis restricted to the 37 patients for whom CD8 IHC staining, bulk RNA-sequencing, and flow cytometry data were all available. In this subset, PD-1 positivity in CD8$^+$ T cells

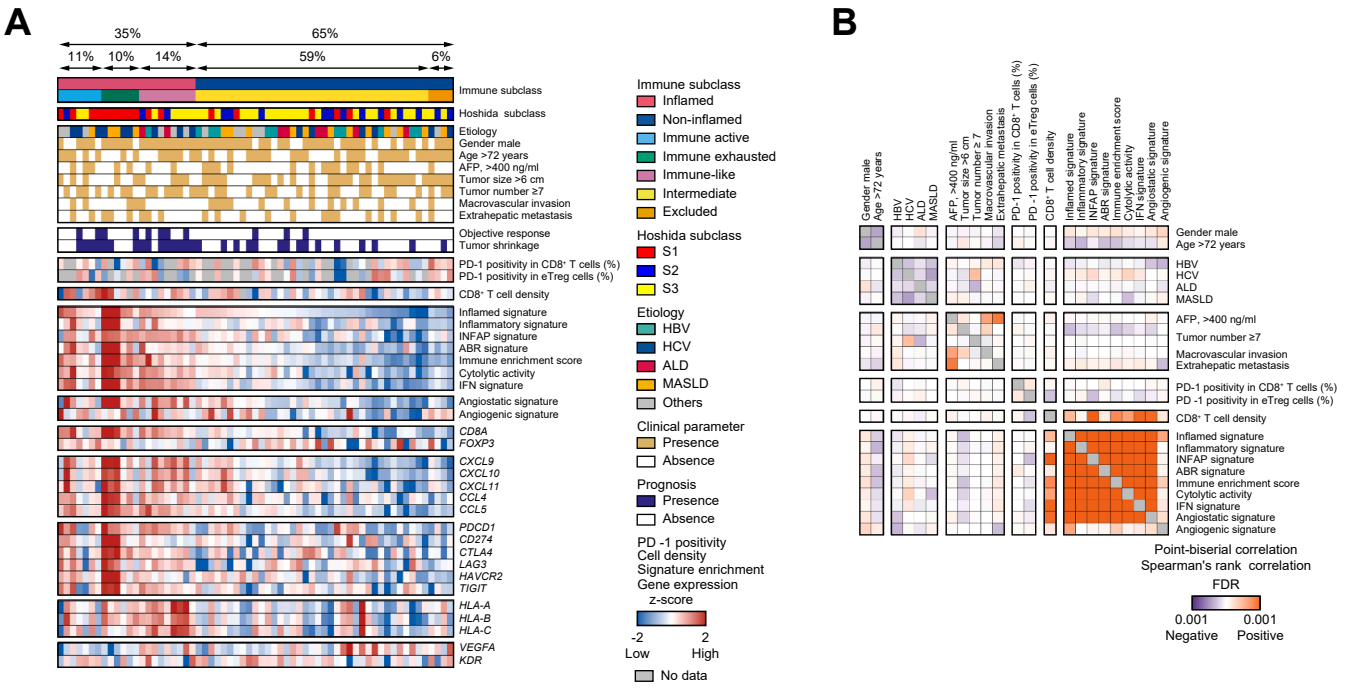

Fig. 1. Association between molecular and immunological features and clinical parameters. (A) Heatmap of molecular and immunological features and clinical parameters (n = 63). Tumor shrinkage was defined as the best tumor lesion response and this was categorized as complete response, partial response, or stable disease with reduction (minor shrinkage within the stable disease range). The heatmap shows the z-scores for PD-1 positivity, cell density, signature enrichment, and gene expression. (B) Correlational heatmap of molecular and immunological features and clinical parameters (n = 63). FDR-adjusted *p* values were calculated using point-biserial correlation for binary variables and Spearman's rank correlation for continuous variables. AFP, alpha-fetoprotein; ALD, alcohol-associated liver disease; eTreg cell, effector regulatory T cell; FDR, false discovery rate; HCC, hepatocellular carcinoma; MASLD, metabolic dysfunction-associated steatotic liver disease; PD-1, programmed death-1.

remained significantly associated with PFS (HR, 0.29; 95% CI, 0.12–0.73), further validating the robustness of our original findings (Fig. S3B).

High PD-1 positivity in CD8$^+$ T cells was associated with favorable PFS independent of CD8$^+$ T-cell density (Fig. 2E). This prompted us to explore the underlying mechanisms that influence treatment efficacy under two contrasting conditions. Using PD-1 positivity in CD8$^+$ T cells as a key indicator, we investigated why some patients showed poor responses despite high CD8$^+$ T-cell density while others achieved favorable responses even with low CD8$^+$ T-cell density.

Spatial analysis of CD8$^+$ T-cell localization and cellular interactions

We first analyzed the relationship between the percentage of PD-1 positivity in CD8$^+$ T cells and immune-related signatures in patients with high CD8$^+$ T-cell density. Gene set enrichment analysis (GSEA) revealed that enrichment of immune-related signatures in samples with high PD-1 positivity in CD8$^+$ T cells (Fig. 3A, Table S3). Further analysis of CD8$^+$ T-cell subtypes previously identified showed enrichment of effector-memory, effector, and cytotoxic T cells in samples with high PD-1 positivity in CD8$^+$ T cells.[25,26] These cells are crucial components of the antitumor response. Conversely, immature subtypes (progenitor and proliferating T cells) were enriched in those with low PD-1 positivity in CD8$^+$ T cells (Fig. 3A, Table S3). To account for potential confounding when inferring immune features from bulk RNA-sequencing data, we compared tumor purity and CD8$^+$ T-cell density between high and low PD-1 positivity groups. Neither showed significant differences (Fig. S4), supporting the validity of our approach for capturing biologically meaningful signals.

These findings led us to hypothesize that CD8$^+$ T cells require a functional antitumor immune response to benefit from Atez/Bev, but that elements of the TME may impair this, even when CD8$^+$ T cells are present within the tumor. Among patients with high CD8$^+$ T-cell density, multiplexed imaging analysis was feasible in three cases. Using these samples, we quantified the cellular interactions between CD8$^+$ T cells and different cell types. Comparative analysis revealed that samples with low PD-1 positivity in CD8$^+$ T cells showed fewer interactions between CD8$^+$ T cells and tumor cells, but more between CD8$^+$ T cells and fibroblasts compared with those with high PD-1 positivity in CD8$^+$ T cells (#48 *vs.* #04 and #39) (Fig. 3B, Fig. S5A). The quantitative spatial analysis further supported this observation, revealing that CD8$^+$ T cells in patients with low PD-1 positivity in CD8$^+$ T cells were located significantly farther from tumor cells (p <0.001) and closer to fibroblasts (p <0.001) than those with high PD-1 positivity in CD8$^+$ T cells (Fig. 3C). Additionally, in the sample from patient #04 with high PD-1 positivity in CD8$^+$ T cells, the CD8$^+$ T cells were predominantly located within the tumor parenchyma, whereas, in the sample from patient #48 with low PD-1 positivity in CD8$^+$ T cells, they were primarily situated in the fibrous stroma (Fig. 3D).

To validate these localization patterns in a larger cohort and establish a clinically applicable method, we further investigated

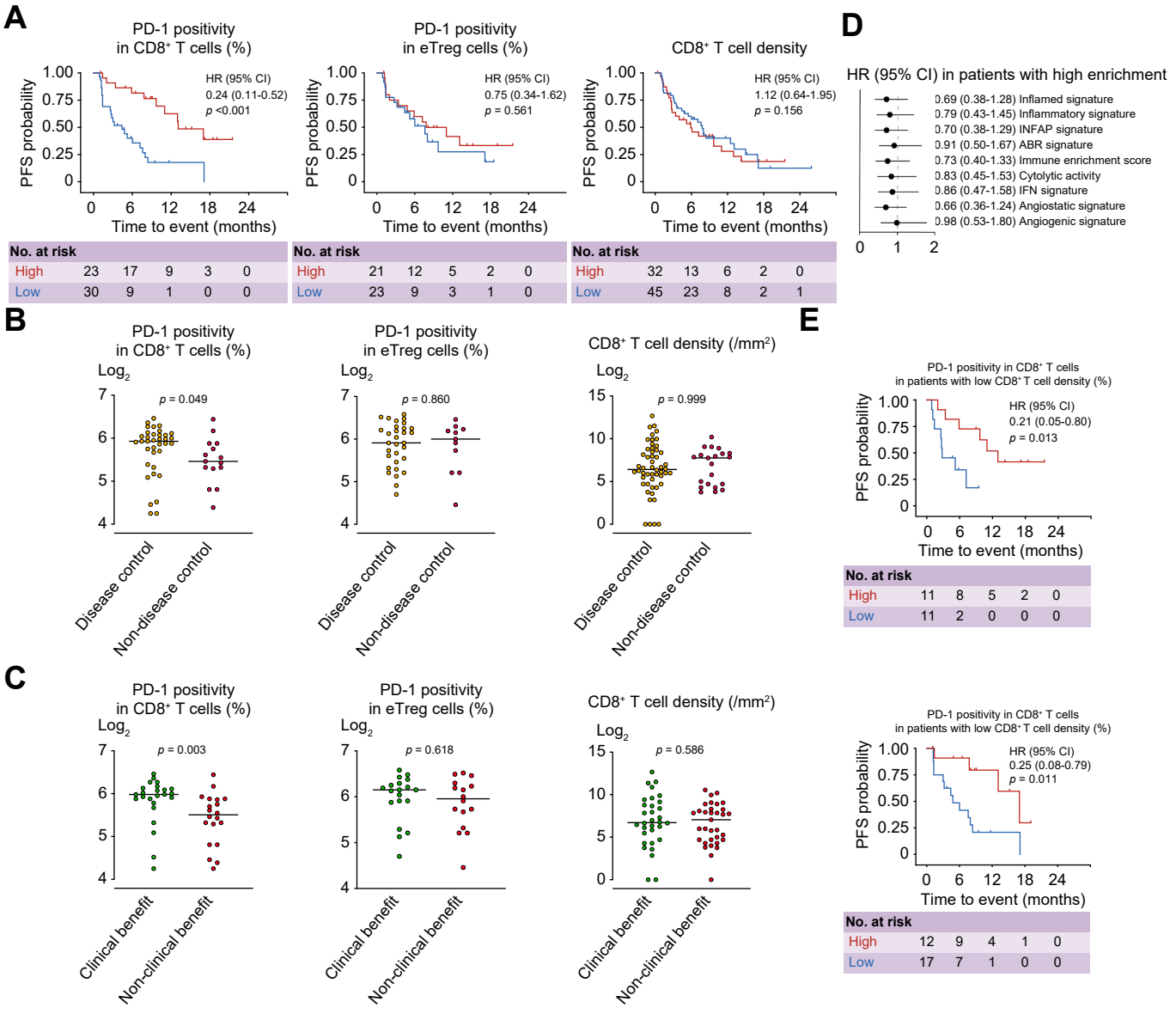

Fig. 2. Association between immunological features and clinical outcomes. (A) PFS analysis of PD-1 positivity in CD8$^+$ T cells (n = 53), PD-1 positivity in eTreg cells (n = 44), and CD8$^+$ T-cell density (n = 77), analyzed by Cox regression model and log-rank test. (B) PD-1 positivity in CD8$^+$ T cells (n = 51), PD-1 positivity in eTreg cells (n = 42), and CD8$^+$ T-cell density (n = 73) in disease control *vs.* non-disease control, analyzed by Wilcoxon rank sum test. (C) PD-1 positivity in CD8$^+$ T cells (n = 44), PD-1 positivity in eTreg cells (n = 35), and CD8$^+$ T-cell density (n = 65) in clinical benefit *vs.* non-clinical benefit, analyzed by Wilcoxon rank sum test. (D) HRs in patients with high enrichment of previously reported immune-related signatures (n = 63), analyzed by Cox regression model. (E) PFS analysis stratified by PD-1 positivity in CD8$^+$ T cells in patients with high (n = 22, top) or low (n = 29, bottom) CD8$^+$ T-cell density, analyzed by Cox regression model and log-rank test. PD-1 positivity in CD8$^+$ T cells, PD-1 positivity in eTreg cells, and immune-related signatures were categorized into high and low based on the median values. CD8$^+$ T-cell density was categorized as high or low using a cut-off of 195 cells/mm^2, as defined in the Supplementary Methods. eTreg cell, effector regulatory T cell; HR, hazard ratio; PD-1, programmed death-1; PFS, progression-free survival.

the CD8$^+$ T-cell localization patterns of 77 tumor biopsy samples, categorizing them as either tumor parenchyma-predominant or fibrous stroma-predominant patterns (see Supplementary Methods) (Fig. 3E). Localization was independently assessed by four investigators. In 11 of 77 cases (14%), discrepancies were resolved by joint review using a multihead microscope. Fleiss' kappa coefficient was 0.828, indicating a high level of inter-observer agreement. Of these, 54 (70%) cases exhibited a tumor parenchyma-predominant pattern, while 23 (30%) showed a fibrous stroma-predominant pattern. Our histological analysis validated the multiplexed imaging findings, demonstrating that patients with a tumor parenchyma-predominant pattern show a better response to Atez/Bev (Fig. 3F) and higher PD-1 positivity in CD8$^+$ T cells (Fig. 3G). This association was confirmed even in patients with high CD8$^+$ T-cell density (Fig. 3H and I), while only a slight similar trend was observed in the low CD8$^+$ T-cell density group (Fig. S6A and B).

To better understand the spatial context of PD-1$^+$ CD8$^+$ T cells, we evaluated interactions and proximity between PD-1$^+$ or PD-1$^-$ CD8$^+$ T cells and fibroblasts, which are predominantly

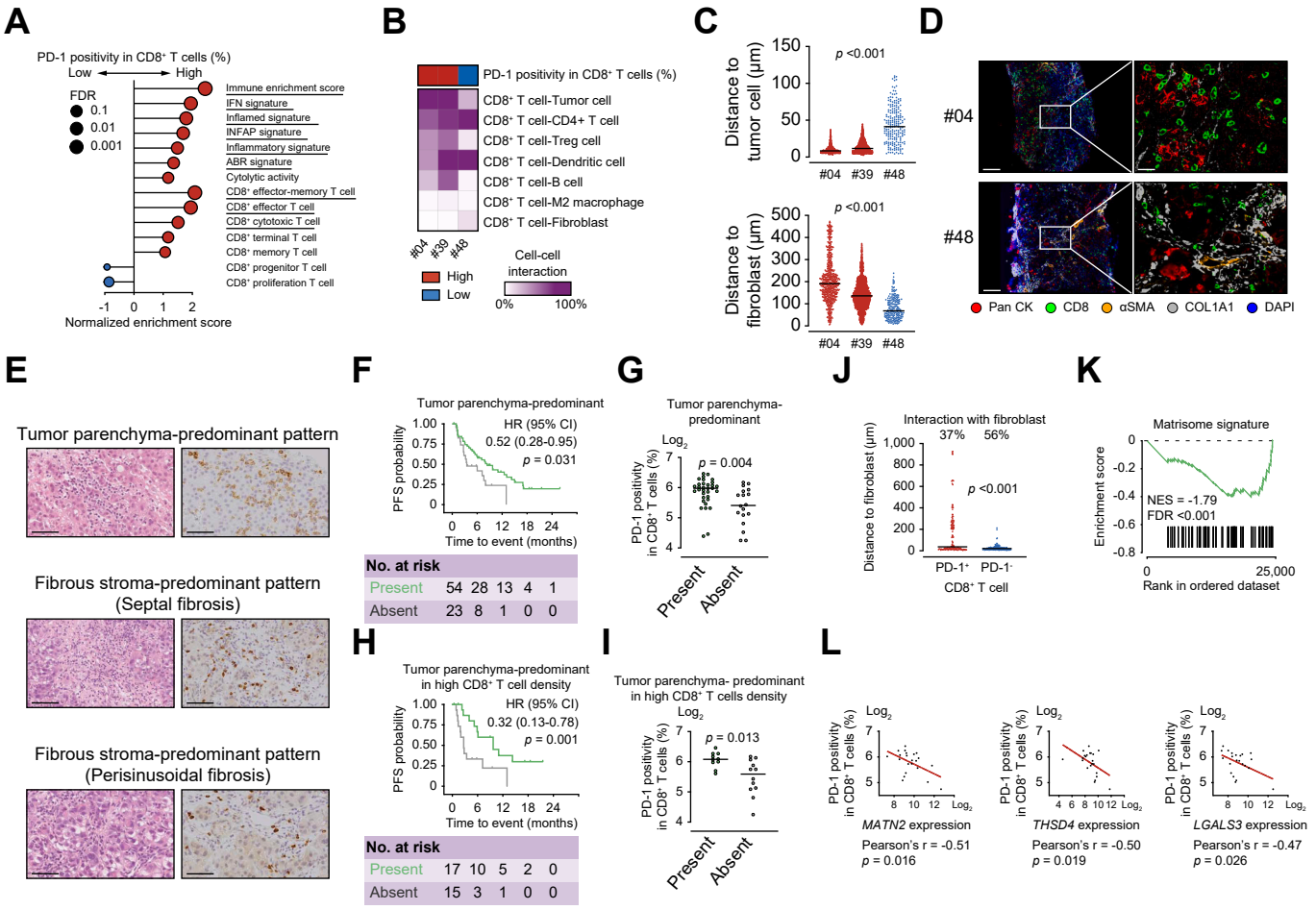

Fig. 3. Impact of spatial localization of CD8⁺ T cells in the therapeutic response. (A) Immune-related signatures and CD8⁺ T-cell subtypes associated with high PD-1 positivity in CD8⁺ T cells (n = 20) by GSEA with FDR adjustment (Benjamini–Hochberg). Gene sets with FDR <0.25 are underlined. (B) Heatmap of cellular interactions between CD8⁺ T cells and other cell types. (C) Minimum distances between CD8⁺ T cells and tumor cells (top) and CD8⁺ T cells and fibroblasts (bottom). Red and blue dots indicate patients with high and low PD-1 positivity in CD8⁺ T cells, respectively. Statistical analysis by Kruskal–Wallis test. (D) Multiplexed images from patients with high (top) and low (bottom) PD-1 positivity in CD8⁺ T cells. The images show five markers (PanCK, CD8, αSMA, COL1A1, and DAPI) overlaid in different colors. Scale bar = 100 μm (left), 20 μm (right). (E) H&E (left) and CD8 IHC (right) images showing tumor parenchyma-predominant and fibrous stroma-predominant patterns. Scale bar = 50 μm. (F) PFS analysis of the tumor parenchyma-predominant pattern (n = 77), analyzed by Cox regression model and log-rank test. (G) PD-1 positivity in CD8⁺ T cells with and without a tumor parenchyma-predominant pattern (n = 51), analyzed by Wilcoxon rank sum test. (H) PFS analysis of the tumor parenchyma-predominant pattern in patients with high CD8⁺ T-cell density (n = 32), analyzed by Cox regression model and log-rank test. (I) PD-1 positivity in CD8⁺ T cells with and without a tumor parenchyma-predominant pattern in patients with high CD8⁺ T-cell density (n = 22), analyzed by Wilcoxon rank sum test. (J) Minimum distances between CD8⁺ T cells and fibroblasts. Red and blue dots indicate PD-1⁺ and PD-1⁻ CD8⁺ T cells, respectively. Statistical analysis by Wilcoxon rank sum test. (K) Association between matrisome signature enrichment and PD-1 positivity in CD8⁺ T cells in patients with high CD8⁺ T-cell density (n = 20) by GSEA with FDR adjustment (Benjamini–Hochberg). (L) Correlation between the expression of each of *MATN2*, *THSD4*, and *LGALS3* and PD-1 positivity in CD8⁺ T cells in patients with high CD8⁺ T-cell density (n = 22), analyzed by Pearson's correlation coefficient. FDR, false discovery rate; HR, hazard ratio; IHC, immunohistochemistry; NES, normalized enrichment score; PD-1, programmed death-1; PFS, progression-free survival; Treg cell, regulatory T cell.

located in the fibrous stroma, in our multiplexed imaging dataset. The results showed that PD-1⁺ CD8⁺ T cells had fewer interactions with fibroblasts and tended to be located farther away from fibroblasts compared with PD-1⁻ CD8⁺ T cells. These findings suggest that PD-1⁺ CD8⁺ T cells preferentially localize to the tumor parenchyma rather than the fibrous stroma, which is consistent with and reinforces our earlier observations (Fig. 3J).

We also examined the matrisome signatures of our samples.[27] This characterizes the tumor-associated fibrous area. Among patients with high CD8⁺ T-cell density, this signature was more enriched in those with lower PD-1 positivity in CD8⁺ T cells (Fig. 3K). Using core enrichment genes, several matrisome genes were identified as significantly negatively correlated with PD-1 positivity in CD8⁺ T cells, including *MATN2* (r = -0.51, p = 0.016), *THSD4* (r = -0.50, p = 0.019), and *LGALS3* (r = -0.47, p = 0.026) (Fig. 3L).

Integrative analysis of CD8⁺ T-cell behavior and the treatment efficacy

We next investigated the mechanisms that enable the therapeutic response to Atez/Bev in patients with low CD8⁺ T-cell density. To explore common features of patients who achieved durable responses and exhibited a high percentage of PD-1 positivity in CD8⁺ T cells regardless of CD8⁺ T-cell density, we analyzed all available samples that met these criteria. Two patients were identified: one had low CD8⁺ T-cell density, and

the other had high CD8$^+$ T-cell density (Fig. S2B). Multiplexed imaging analysis revealed that the patient with a low CD8$^+$ T-cell density (#26) showed a cellular interaction pattern similar to that in the patient with a high CD8$^+$ T-cell density (#39) (Fig. 4A). Both patients demonstrated numerous interactions between tumor cells, CD4$^+$ T cells, and dendritic cells, but few between CD8$^+$ T cells and fibroblasts. This reinforced our previous finding that the absence of fibroblast interaction may be crucial for the therapeutic efficacy of Atez/Bev.

To further understand the treatment response in this patient with low CD8$^+$ T-cell density, we analyzed temporal changes in the TME based on both baseline and in-treatment biopsy samples, which provided a rare opportunity in advanced HCC. Both biopsies were obtained from the same tumor lesion, allowing for a direct comparison of the TME baseline and in-treatment. Despite radiological evidence suggesting tumor enlargement, the patient showed a rapid decrease in AFP levels 2 months after treatment initiation (Fig. 4B). An in-treatment biopsy obtained during this period proved valuable as the tumor subsequently shrank, confirming pseudoprogression. The patient achieved cancer-free status following surgical resection of a single remaining nodule, providing unique insights into TME dynamics during successful Atez/Bev treatment. The baseline and in-treatment CD8 IHC staining results are shown in Fig. 4C. Although the CD8$^+$ T-cell density was low at baseline, a remarkable increase in CD8$^+$ T-cell density was observed after treatment initiation. Multiplexed imaging analysis showed increased PD-1$^+$ CD8$^+$ T cells (Fig. 4D and E) and increased interaction between CD8$^+$ T cells and other cells, including tumor cells, CD4$^+$ T cells, and dendritic cells (Fig. 4F). These findings were further validated by bulk RNA-sequencing deconvolution analysis, which confirmed the increased abundance of CD8$^+$ T cells, CD4$^+$ T cells, and dendritic cells in-treatment (Fig. 4G). Notably, CD8 IHC imaging revealed an intriguing pattern at baseline. Despite their low CD8$^+$ T-cell density, the CD8$^+$ T cells exhibited diffuse distribution throughout the tumor parenchyma rather than focal clustering (Fig. 4C).

Spatial dynamics of CD8$^+$ T cells and clinical outcome of combined treatment with Atex/Bev in patients with advanced HCC

Based on these observations of the diffuse CD8$^+$ T-cell distribution pattern in a responding patient, we systematically analyzed the spatial distribution patterns of CD8$^+$ T cells within the tumor parenchyma using routine H&E and CD8 IHC staining. We classified these patterns as either diffuse or localized (see Supplementary Methods). Representative images of distribution patterns are provided in Fig. 5A. We found a diffuse distribution pattern in 38 cases and a localized distribution pattern in 39 cases. Patients whose tumors showed diffuse CD8$^+$ T-cell distribution within the tumor parenchyma demonstrated both better responses to Atez/Bev (Fig. 5B) and higher PD-1 positivity in CD8$^+$ T cells (Fig. 5C). This was true even in patients with low CD8$^+$ T-cell density (Fig. 5D and E), while only a slight similar trend was observed in high CD8$^+$ T-cell density group (Fig. S6C and D).

Given that patients who showed a durable response and had high PD-1 positivity in CD8$^+$ T cells did not show any interaction between CD8$^+$ T cells and fibroblasts (Fig. 4A), we investigated whether CD8$^+$ T-cell interactions with fibroblasts might prevent the diffuse distribution of CD8$^+$ T cells across the tumor parenchyma. To address this, we analyzed all nine patients for whom CD8$^+$ T-cell distribution could be evaluated. Our analysis revealed more frequent CD8$^+$ T-cell–fibroblast interactions with localized distribution than those with diffuse distribution (Fig. 5F). We further quantified this observation by measuring the spatial proximity between these cell types, confirming that CD8$^+$ T cells and fibroblasts were significantly closer to each other with localized distribution (Fig. 5G).

Through our spatial analyses and conventional histological assessment using H&E and CD8 IHC staining, we identified two key determinants of the response to Atez/Bev. These were the preferential localization of CD8$^+$ T cells to the tumor parenchyma over the fibrous stroma and their distribution pattern within the tumor parenchyma. By integrating these spatial features, we found that patients whose tumors exhibited both favorable features (CD8$^+$ T cells predominantly localizing to the tumor parenchyma and showing diffuse distribution within the tumor parenchyma) were more likely to show high PD-1 positivity in CD8$^+$ T cells (83%) and achieved the longest median PFS (14.3 months; log-rank, $p = 0.019$) (Fig. 5H and I). Compared with the rest of the cohort, patients with both favorable features had a reduced risk of progression (HR 0.37; 95% CI 0.19–0.73), which remained significant after adjustment for potential prognostic clinical variables (Table S4). Notably, these two infiltration patterns showed no clear association with elevated AFP levels (>400 ng/ml); the odds ratio was 0.55 ($p = 0.283$) for the tumor parenchyma-predominant pattern and 1.17 ($p = 0.807$) for the diffuse distribution pattern.

To validate these findings, we analyzed an independent cohort of 25 patients with advanced HCC who received Atez/Bev and had baseline biopsy samples available (details regarding clinical characteristics and treatment outcomes are provided in the Supplementary Results). Patients in the validation cohort whose tumors also showed CD8$^+$ T cells predominantly localized to and diffusely distributed within the tumor parenchyma demonstrated a trend toward improved PFS, consistent with the derivation cohort (HR, 0.12; 95% CI, 0.00–0.94; log-rank, $p = 0.047$) (Fig. 5J).

Dual regulation of effector CD8$^+$ T cells and eTreg cells by combined treatment with Atez/Bev

In HCC, regulatory T cells (Treg) cells are associated with poor clinical outcomes in patients receiving anti-PD-1 or anti-PD-L1 monotherapy, a pattern consistently observed across multiple cancer types.[10,28,29] Therefore, understanding the functional interplay between CD8$^+$ T cells and Treg cells is crucial for characterizing the TME of advanced HCC. Our spatial analyses revealed an intriguing relationship between CD8$^+$ T cells and Treg cells. Specifically, when tumors exhibit high infiltration of PD-1$^+$ CD8$^+$ T cells, interactions between CD8$^+$ T cells and Treg cells were more frequently observed, as shown in Fig. 3B. This suggests the concurrent recruitment of CD8$^+$ T cells and Treg cells in advanced HCC. Although previous studies have shown that PD-1 or PD-L1 blockade can activate both effector CD8$^+$ T cells and eTreg cells,[14,15] we found no correlation between high percentage of PD-1 positivity in eTreg cells and poor clinical outcomes in patients treated with Atez/Bev. This finding led us to hypothesize that Bev may counteract the potentially negative effects of PD-L1 blockade on eTreg-cell activation.

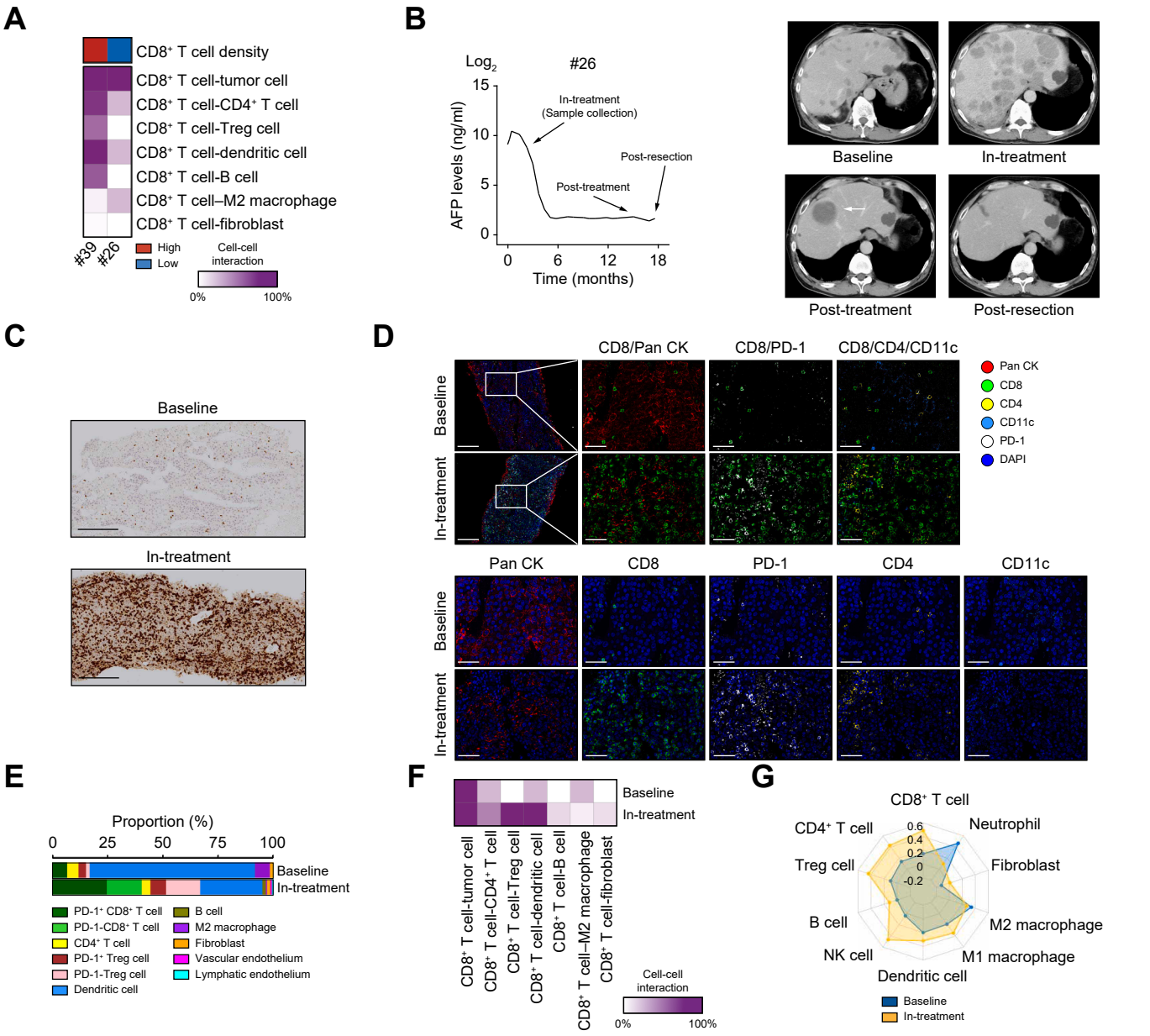

Fig. 4. Dynamic changes in the tumor microenvironment of advanced hepatocellular carcinoma during successful atezolizumab plus bevacizumab combination therapy. (A) Heatmap of cellular interactions between CD8⁺ T cells and other cell types. (B) Changes in AFP levels (left) and CT images (right) during Atez/Bev in patient #28. A white arrow indicates a single remaining nodule. (C) CD8 IHC images at baseline and in-treatment in patient #28. Scale bar = 200 μm. (D) Multiplexed images at baseline and in-treatment in patient #28. Images show six markers (PanCK, CD8, CD4, CD11c, PD-1, and DAPI) overlaid in different colors. Scale bar = 200 μm (row 1 and 2, columns 1), 50 μm (others). (E) Distribution of cell types at baseline and in-treatment in patient #28. (F) Heatmap of cellular interactions between CD8⁺ T cells and other cell types at baseline and in-treatment in patient #28. (G) Relative abundance of cell types at baseline and in-treatment in patient #28. AFP, alpha-fetoprotein; Atez, atezolizumab; Bev, bevacizumab; CT, computed tomography; IHC, immunohistochemistry; PD-1, programmed death-1; Treg cell, regulatory T cell.

To evaluate the mechanistic contribution of Bev in the Atez/Bev regimen, we analyzed patients with available baseline flow cytometry data who underwent Bev interruption and continued treatment with Atez monotherapy. In all six cases, Bev was discontinued because of adverse events, most commonly proteinuria, which is a frequent cause of treatment modification in clinical practice.[5,30] In these patients, Atez was maintained as monotherapy. Treatment was ultimately discontinued upon radiologic disease progression, characterized by the enlargement of existing lesions rather than the development of new lesions (Table S5). Among these patients, those with high PD-1 positivity in eTreg cells demonstrated a trend toward shorter times to disease progression after Bev interruption than those with low PD-1 positivity in eTreg cells (Fig. 6A). To further characterize the impact of Bev interruption, we performed multiplexed imaging analysis on paired tumor samples obtained at baseline and post-progression. Two patients met the criteria for this analysis, and both were included as representative

cases with different clinical courses. Patient #85 progressed after switching to Atez monotherapy because of Bev interruption, while patient #65 progressed during ongoing combination therapy without interruption. The clinical trajectories of these two patients are illustrated in Fig. 6B. In patient #85, we observed accelerated tumor growth rates on computed

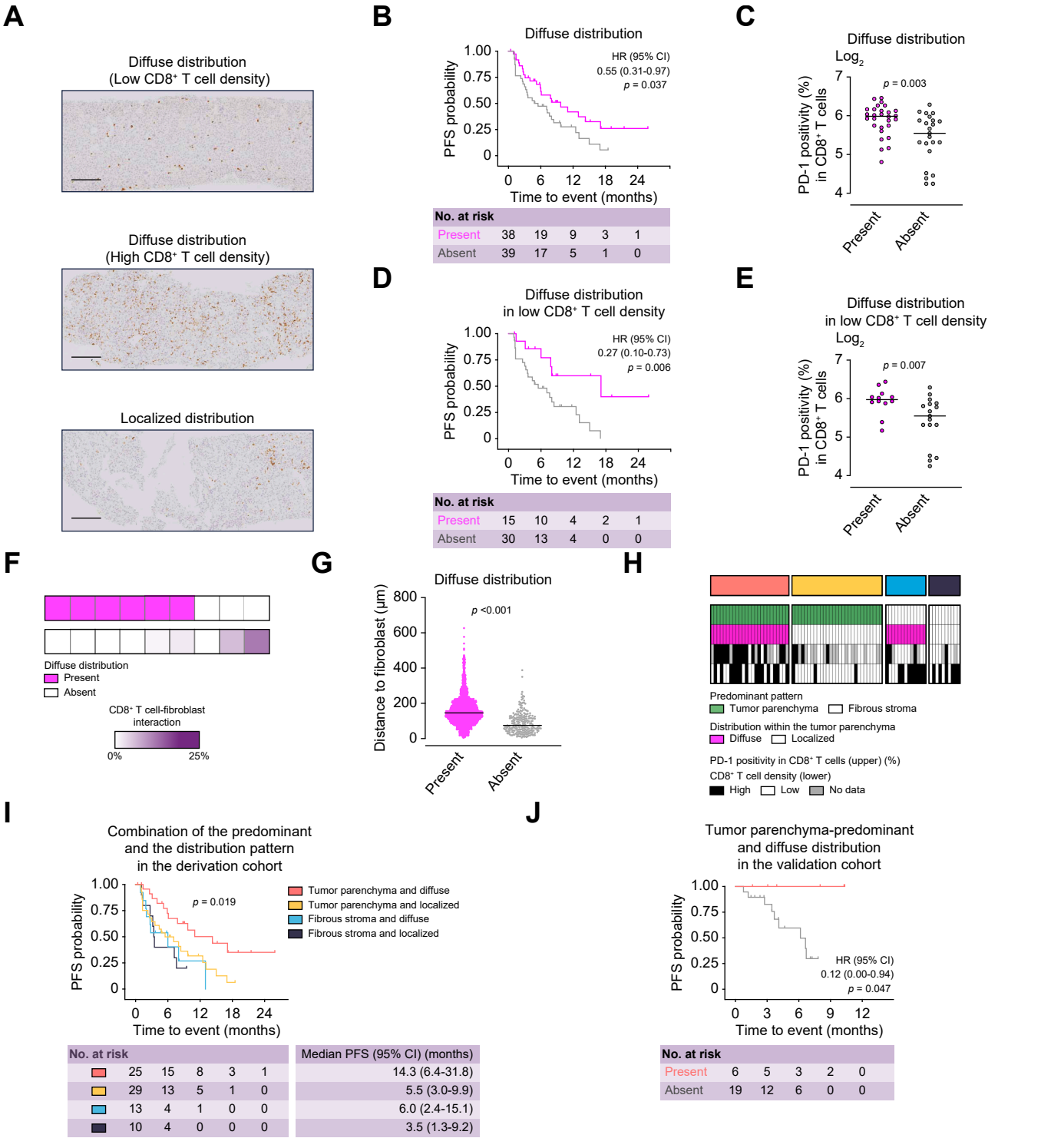

Fig. 5. Significance of the diffuse distribution of CD8⁺ T cells within the tumor parenchyma in favorable treatment response. (A) CD8 IHC images showing the distribution patterns within the tumor parenchyma. Diffuse distribution was defined as the presence of three or more CD8⁺ T cells throughout all contiguous tumor parenchyma in a high-power field, while localized distribution did not meet this criterion. Scale bar = 100 μm. (B) PFS analysis of the diffuse distribution pattern within the tumor parenchyma (n = 77), analyzed by Cox regression model and log-rank test. (C) PD-1 positivity in CD8⁺ T cells with and without diffuse distribution within the tumor parenchyma (n = 51), analyzed by Wilcoxon rank sum test. (D) PFS analysis of the distribution patterns within the tumor parenchyma of patients with low CD8⁺

tomography imaging (Fig. S7). Furthermore, this patient showed significantly increased PD-1 positivity in Treg cells at progression compared with baseline (Fig. 6C and D).

GSEA comparing baseline and post-progression samples revealed marked differences between patients who experienced disease progression after moving to Atez monotherapy, and those who experienced disease progression with ongoing Atez/Bev (Table S6 and S7). Key pathways associated with antitumor immune activity, including interferon-gamma responses, were notably suppressed at progression in patients whose disease progressed after Bev interruption. In contrast, these pathways were maintained in patients whose disease progressed without Bev interruption, as illustrated in Fig. 6E. These findings suggest that the loss of the suppressive effects of Bev on Treg cells may reduce CD8$^+$ T-cell activity and lead to disease progression. As an additional note, the inhibition of tumor angiogenesis is among the known antitumor mechanisms of Bev.[31] To further explore this association, the angiostatic signature, angiogenic signature, and vascular endothelial growth factor (*VEGF*) expression were individually assessed in patients who experienced disease progression following Bev interruption. A shorter interval from Bev discontinuation to disease progression was observed in patients with low angiostatic signatures, or with high angiogenic signatures or *VEGF* expression, compared with those with the opposite profiles (Fig. S8). In the GSEA comparison, there was greater activation of angiogenesis-related pathways in patients whose disease progressed after Bev interruption than in those whose disease progressed without Bev interruption, although this difference was not statistically significant.

Building on these findings, the immunological effects of Bev were subsequently evaluated using an *in vitro* model designed to minimize the contribution of vascular endothelial cells. We examined the effects of Atez alone and in combination with Bev on eTreg-cell activation. Peripheral blood mononuclear cells treated with Atez alone showed increased expression of eTreg-cell activation markers, including PD-1, CTLA-4, ICOS, and GITR. The addition of Bev suppressed the expression of these activation markers, as shown in Fig. 6F. These results support the hypothesis that Bev mitigates the eTreg-cell activation induced by PD-L1 blockade.

Discussion

Our analysis of the TME in patients with advanced HCC treated with Atez/Bev revealed that while the percentage of PD-1 positivity in CD8$^+$ T cells predicts treatment efficacy,[14,15] CD8$^+$ T-cell density proved insufficient as a predictive marker, aligning with recent studies.[26,32] Using PD-1 positivity in CD8$^+$ T cells as a key indicator, our detailed spatial analysis identified two critical determinants of therapeutic response: CD8$^+$ T cells must be localized within the tumor parenchyma rather than the fibrous stroma, and maintain diffuse distribution throughout the tumor parenchyma. These spatial features correlated with higher PD-1 positivity in CD8$^+$ T cells and improved outcomes. Importantly, these characteristics can be evaluated through conventional histological assessment, enabling practical implementation in clinical settings. IHC is a widely used and accessible technique in routine pathology, and CD8 is among the most commonly used and well-validated antibodies. The evaluation criteria we proposed represent a simple and broadly applicable method, allowing pathologists to score the localization and distribution of CD8$^+$ T cells in <1 min per sample without the need for any specialized digital pathology tools, making this approach highly suitable for widespread clinical implementation. Nevertheless, we recognize that the predictive value of CD8$^+$ T-cell-based histological biomarkers requires further validation. While we conducted an independent validation, confirmation in larger and independent cohorts is essential to establish their clinical applicability. The lack of robust external validation remains a major limitation of this study.

Our findings suggest that fibroblasts, which are one of the main components of the fibrous stroma, play a crucial role in regulating CD8$^+$ T-cell behavior.[33] Exploring the molecular basis of these observations, we identified several matrisome genes whose presence was negatively correlated with PD-1 positivity in CD8$^+$ T cells. Notably, *LGALS3*, which encodes galectin-3, a protein known to suppress CD8$^+$ T cells via T-cell receptor signaling and activate fibroblasts.[34–36] Given its ability to bind to both extracellular matrix components and CD8$^+$ T cells,[37] galectin-3 may contribute to the retention of CD8$^+$ T cells within the fibrous stroma while simultaneously suppressing their activity through T-cell receptor-mediated mechanisms and fibroblasts. Targeting fibroblast-mediated immunosuppression could enhance the efficacy of immunotherapy in advanced HCC. However, our findings suggest that the presence of fibrous stroma alone is not sufficient to define an immunosuppressive microenvironment, as only ∼40% of patients with fibrous stroma exhibited a fibrous stroma-predominant CD8$^+$ T-cell localization pattern. Therefore, stroma-targeting strategies may be most beneficial in patients whose CD8$^+$ T cells are sequestered within fibrotic regions. Further studies are warranted to identify the patient subgroups that would derive the greatest benefit from such approaches.

Previous immunotherapy-related biomarker studies have predominantly used quantitative assessments.[8,38] Recent studies have demonstrated that CD8$^+$ T cells must undergo local differentiation and expansion within the tumor for effective immunotherapy responses,[26] and that spatial organization of immune cells within the TME is important for therapeutic

T-cell density (n = 45), analyzed by Cox regression model and log-rank test. (E) PD-1 positivity in CD8$^+$ T cells with and without diffuse distribution within the tumor parenchyma in patients with low CD8$^+$ T-cell density (n = 29), analyzed by Wilcoxon rank sum test. (F) Heatmap of cellular interactions between CD8$^+$ T cells and fibroblasts. (G) Minimum distances between CD8$^+$ T cells and fibroblasts. Pink and gray dots indicate patients with and without diffuse distribution within the tumor parenchyma, respectively. Statistical analysis by Wilcoxon rank sum test. (H) Heatmap of the predominant pattern, distribution pattern within the tumor parenchyma, PD-1 positivity in CD8$^+$ T cells, and CD8$^+$ T-cell density (n = 77). (I) PFS analysis of the combination of the predominant pattern and the distribution pattern within the tumor parenchyma in the derivation cohort (n = 77), analyzed by log-rank test. Each color represents a combination of spatial features: pink for tumor parenchyma-predominant with diffuse distribution, yellow for tumor parenchyma-predominant with localized distribution, blue for fibrous stroma-predominant with diffuse distribution, and navy for fibrous stroma-predominant with localized distribution. (J) PFS analysis of tumor parenchyma-predominant and diffuse distribution in the validation cohort (n = 25), analyzed by Cox regression model and log-rank test. HR, hazard ratio; IHC, immunohistochemistry; PD-1, programmed death-1; PFS, progression-free survival.

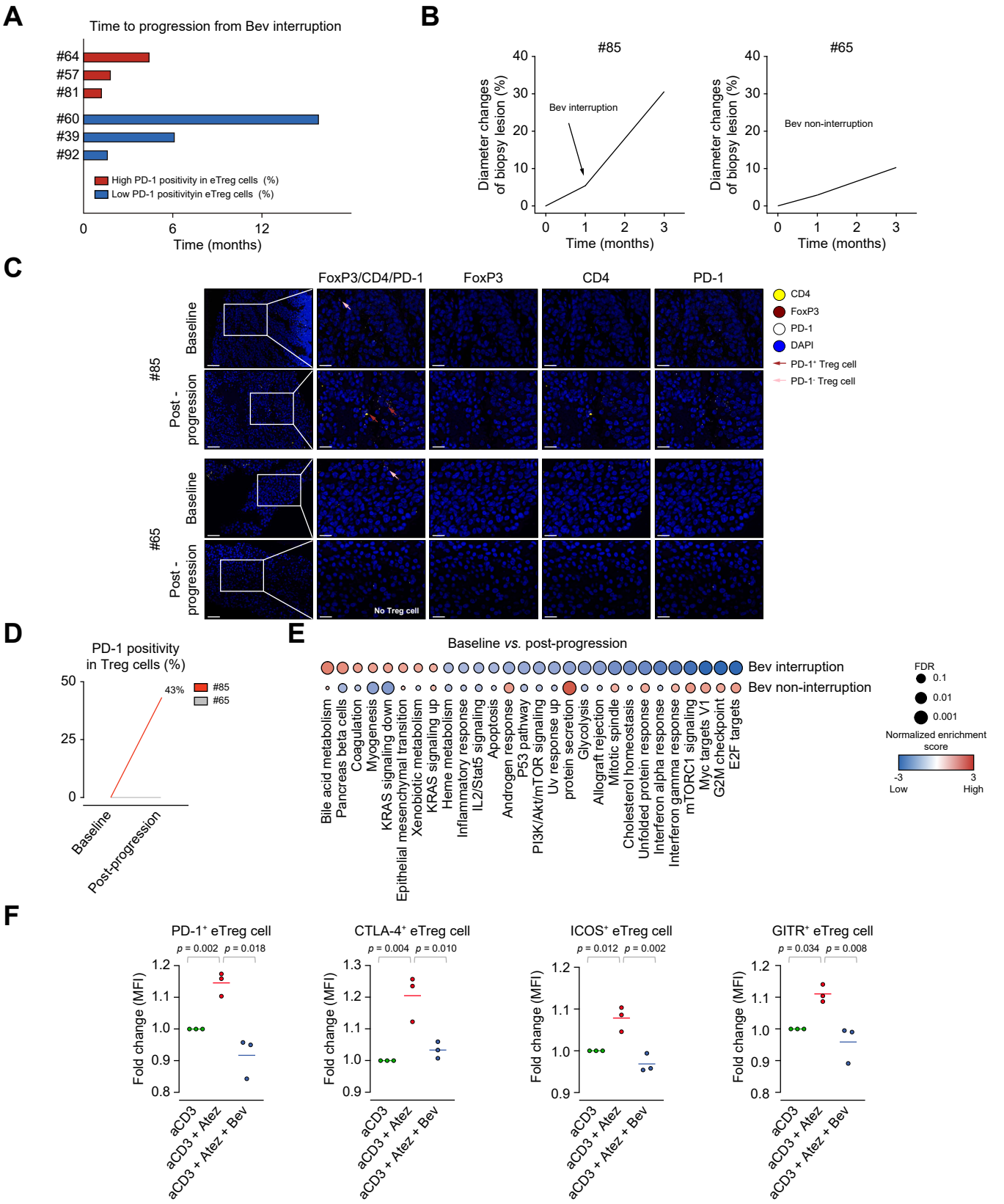
A
Time to progression from Bev interruption
#64
#57
#81
#60
#39
#92
High PD-1 positivity in eTreg cells (%)
Low PD-1 positivityin eTreg cells (%)
0
6
12
Time (months)
B
#85
Bev interruption
Diameter changes of biopsy lesion (%)
Time (months)
#65
Bev non-interruption
C
FoxP3/CD4/PD-1
FoxP3
CD4
PD-1
#85
#65
Baseline
Post - progression
No Treg cell
CD4
FoxP3
PD-1
DAPI
PD-1+ Treg cell
PD-1- Treg cell
D
PD-1 positivity in Treg cells (%)
43%
#85
#65
Baseline
Post-progression
E
Baseline vs. post-progression
Bev interruption
Bev non-interruption
Bile acid metabolism
Pancreas beta cells
Coagulation
Myogenesis
KRAS signaling down
Epithelial mesenchymal transition
Xenobiotic metabolism
KRAS signaling up
Heme metabolism
Inflammatory response
IL2/Stat5 signaling
Apoptosis
Androgen response
P53 pathway
PI3K/Akt/mTOR signaling
Uv response up
protein secretion
Glycolysis
Allograft rejection
Mitotic spindle
Cholesterol homeostasis
Unfolded protein response
Interferon alpha response
Interferon gamma response
mTORC1 signaling
Myc targets V1
G2M checkpoint
E2F targets
FDR
0.1
0.01
0.001
Normalized enrichment score
-3
3
Low
High
F
PD-1+ eTreg cell
p = 0.002
p = 0.018
CTLA-4+ eTreg cell
p = 0.004
p = 0.010
ICOS+ eTreg cell
p = 0.012
p = 0.002
GITR+ eTreg cell
p = 0.034
p = 0.008
Fold change (MFI)
aCD3
aCD3 + Atez
aCD3 + Atez + Bev

outcomes.[26,32] Our spatial analysis between fibrous components and CD8$^+$ T cells revealed patterns critical to immunotherapy outcomes. Our spatial approach also provided novel insights into pseudoprogression, as evidenced by cases where tumor enlargement was accompanied by increased CD8$^+$ T-cell infiltration with maintained favorable distribution patterns following Atez/Bev. Although biopsy samples represent only a limited portion of the tumor, previous studies have demonstrated that they reflect the immunophenotypic characteristics of the tumor as a whole with ~75% accuracy, supporting their use as a reliable proxy for evaluating the TME.[39] Furthermore, the consistency observed between our derivation cohort and validation cohort supports the robustness of our preliminary findings and reinforces the utility of single-tumor biopsy analysis. In the derivation cohort, two cases had multiple biopsy samples taken from different regions of the same tumor nodule, and the localization and distribution pattern of CD8$^+$ T cells, as defined in our study, were consistent across these regions (Fig. S9). While further investigation with larger numbers of spatially distinct samples is warranted, these findings reinforce the validity of using single biopsy samples to assess immune-cell distribution within tumors. Given that differences in sample numbers across platforms may raise concerns about data integrity, these discrepancies primarily reflect the limited quantity of biopsy material and its sequential allocation across assays. This limitation is inherent to studies of advanced HCC, where tissue resection is often not feasible and biopsies frequently represent the only available material for analysis. Nonetheless, recent studies have demonstrated that biopsy-based multiplatform analyses can yield meaningful immunological insights,[40] underscoring both the feasibility and importance of this approach. Optimizing strategies to derive maximal biological insight from limited tissue material remains an important area for future investigation.

In contrast to our findings with CD8$^+$ T cells, the predictive value of the percentage of PD-1 positivity in eTreg cells diverged from the findings of previous studies of other cancer types.[14,15] We attribute this to the presence of Bev in our treatment regimen, revealing a novel mechanistic interaction between VEGF and anti-PD-L1 therapies. The role of VEGF in activating immunosuppressive cells, including Treg cells, and the suppressive effect of Bev on Tregs in advanced HCC have previously been established.[10,13,41] The present study uniquely demonstrates how an anti-VEGF antibody can counterbalance the potentially deleterious effects of PD-L1 blockade by suppressing eTreg-cell activation. This finding expands our understanding of the effects of combination immunotherapies in HCC. However, further research is needed to determine whether Bev directly suppresses the activation of eTreg cells within tumors, and whether the suppression of eTreg-cell activation by Bev contributes to improved clinical outcomes.

In conclusion, our study presents two major findings regarding the treatment of advanced HCC with Atez/Bev. First, we demonstrate that conventional histological assessment of the spatial characteristics of CD8$^+$ T cells, including their localization and distribution pattern within the tumor parenchyma can serve as a predictor of treatment efficacy. This provides an easily applicable tool for more informed clinical decision-making. Second, we uncovered a novel synergistic mechanism in Atez/Bev, whereby the suppression of eTreg-cell activation by Bev enhances the efficacy of PD-L1 blockade. These findings not only provide a framework for biomarker-guided patient selection but also offer mechanistic insights that can inform the design of future immunotherapy combinations for advanced HCC. This is an exploratory analysis with no current consequences in clinical practice. Future studies should confirm the results in an external cohort.

Affiliations

[1]*Department of Gastroenterology, Graduate School of Medicine, Chiba University, Chiba, Japan;* [2]*Division of Digestive and Liver Diseases, Department of Internal Medicine, The University of Texas Southwestern Medical Center, Dallas, TX, USA;* [3]*Department of Tumor Microenvironment, Graduate School of Medicine, Dentistry and Pharmaceutical Sciences, Okayama University, Okayama, Japan;* [4]*Department of General Surgery, Graduate School of Medicine, Chiba University, Chiba, Japan;* [5]*Division of Cell Therapy, Chiba Cancer Center Research Institute, Chiba, Japan;* [6]*Department of Diagnostic Pathology, Graduate School of Medicine, Chiba University, Chiba, Japan;* [7]*Department of Pathology, International University of Health and Welfare, School of Medicine, Narita Hospital, Chiba, Japan;* [8]*Department of Allergy and Respiratory Medicine, Okayama University Hospital, Okayama, Japan;* [9]*Kindai University Faculty of Medicine, Osaka, Japan*

Abbreviations

AFP, alpha-fetoprotein; ALD, alcohol-associated liver disease; Atez, atezolizumab; Bev, bevacizumab; eTreg, effector regulatory T cell; GSEA, gene set enrichment analysis; HCC, hepatocellular carcinoma; HR, hazard ratio; IHC, immunohistochemistry; MASLD, metabolic dysfunction-associated steatotic liver disease; MFI, mean fluorescent intensity; NES, normalized enrichment score; PD-1, programmed death-1; PD-L1, programmed death-ligand 1; PFS, progression-free survival; TME, tumor microenvironment; Treg, regulatory T cell; VEGF, vascular endothelial growth factor.

Conflicts of interest

SO received honoraria from Eisai, Chugai Pharmaceutical, AstraZeneca, and Merck & Co., Inc.; consulting or advisory fees from Eisai, Merck & Co., Inc., Chugai Pharmaceutical, and AstraZeneca; and research grants from Bayer, AstraZeneca, Chugai Pharmaceutical, and Eisai. JL received research grants from Taiju Life Social Welfare Foundation and, in the form of computing hardware, NVIDIA Corporation outside of this study. YH advises and owns stock in Alentis Therapeutics and Espervita Therapeutics. He advises Helio Genomics, Roche Diagnostics, and Elevar Therapeutics. MKom received honoraria from

Fig. 6. Effects of bevacizumab interruption on effector regulatory T-cell activation. (A) Associations between PD-1 positivity in eTreg cells and time to progression after Bev interruption. (B) Changes in biopsy lesion diameter during Atez/Bev in patients #85 (left) and #65 (right). (C) Multiplexed images at baseline and post-progression in patient #85 (top) and #65 (bottom). Images show four markers (CD4, FoxP3, PD-1, and DAPI) overlaid in different colors. Scale bar = 50 μm (far left), 20 μm (others). (D) PD-1 positivity in Treg cells at baseline and post-progression in patients #85 (red line) and #65 (gray line). (E) Comparison of the changes in the hallmark molecular pathways after disease progression in the Bev interruption (n = 3) *vs.* Bev non-interruption groups (n = 3) by GSEA with FDR adjustment (Benjamini–Hochberg). The gene sets with FDR <0.25 in the Bev interruption group were included. If more than 20 pathways met this criterion, only the top 20 pathways were shown, according to NES. (F) Comparison of the fold changes in the MFI of eTreg-cell activation markers (PD-1, CTLA-4, ICOS, and GITR) between Atez alone and Atez/Bev groups (n = 3 per group), analyzed by Bonferroni-adjusted *t* tests. Atez, atezolizumab; Bev, bevacizumab; eTreg cell, effector regulatory T cell; FDR, false discovery rate; MFI, mean fluorescent intensity; NES, normalized enrichment score; PD-1, programmed death-1; Treg cell, regulatory T cell.

Eisai outside of this study. YTog received institutional research funding and honoraria from Ono Pharmaceutical, Bristol-Myers Squibb, AstraZeneca, and Chugai Pharmaceutical; research grants from Daiichi-Sankyo, Janssen Pharmaceutical, KOTAI, KORTUC, Takeda, and Taiho; and honoraria from Eisai and MSD outside of this study. The remaining authors have no conflicts to report.

Please refer to the accompanying ICMJE disclosure forms for further details.

Authors' contributions

Conceptualization and data interpretation: HK, TI, SO, MKom, YTog. Data collection: HK, TI, SO, TTsu, MF, MS, RI, TA, CM, TY, SY, MNakag, RK, KKor, MI, KKob, NK, MNakam, TK, SN, TTak, YTak, KT, JI, MO, MKom. Data analysis: HK, TI, SO, JL, MKaw, MKom. Manuscript writing: HK, SO. Supervision: SO, YH, MKom, YTog. Critically reviewed the report, offered feedback on drafts, and approved the final manuscript: all authors.

Data availability

All data generated or analyzed during this study are included in this article and its online supplementary material files. The RNA-sequencing dataset is publicly available at NCBI GEO (accession numbers: GSE285963). Further enquiries can be directed to the corresponding author.

Declaration of generative AI and AI-assisted technologies in the writing process

During the preparation of this work the authors used ChatGPT in order to assist with English proofreading. After using this tool/service, the authors reviewed and edited the content as needed and take full responsibility for the content of the publication.

Financial support

This study was funded by Chugai Pharmaceutical Co., Ltd and partially supported by JSPS KAKENHI Grant Number 22K08049.

Acknowledgments

We extend our sincere gratitude to Satomi Nakamura, Yuka Iwase, and Ryoko Arai for their invaluable contributions to data management. We also thank Risa Kakiuchi, Etsuko Tanji, Yuki Nakamura, and Momoko Iwatsuru for their assistance with the experiments. The authors would like to acknowledge Enago (www.enago.jp) for their support with the English-language review. Additionally, we appreciate BioRender (BioRender.com) for providing the tools used to create one of the figures and the graphical abstract in this manuscript.

Supplementary data

Supplementary data to this article can be found online at https://doi.org/10.1016/j.jhepr.2025.101614.

References

Author names in bold designate shared co-first authorship

[1] Sung H, Ferlay J, Siegel RL, et al. Global Cancer Statistics 2020: GLOBOCAN estimates of incidence and mortality worldwide for 36 cancers in 185 countries. CA Cancer J Clin 2021;71:209–249.
[2] Siegel RL, Giaquinto AN, Jemal A. Cancer statistics, 2024. CA Cancer J Clin 2024;74:12–49.
[3] Rumgay H, Arnold M, Ferlay J, et al. Global burden of primary liver cancer in 2020 and predictions to 2040. J Hepatol 2022;77:1598–1606.
[4] Singal AG, Kanwal F, Llovet JM. Global trends in hepatocellular carcinoma epidemiology: implications for screening, prevention and therapy. Nat Rev Clin Oncol 2023;20:864–884.
[5] Finn RS, Qin S, Ikeda M, et al. Atezolizumab plus bevacizumab in unresectable hepatocellular carcinoma. N Engl J Med 2020;382:1894–1905.
[6] Gordan JD, Kennedy EB, Abou-Alfa GK, et al. Systemic therapy for advanced hepatocellular carcinoma: ASCO guideline update. J Clin Oncol 2024;42:1830–1850.
[7] de Visser KE, Joyce JA. The evolving tumor microenvironment: from cancer initiation to metastatic outgrowth. Cancer Cell 2023;41:374–403.
[8] **Zhang N**, **Yang X**, **Piao M**, et al. Biomarkers and prognostic factors of PD-1/PD-L1 inhibitor-based therapy in patients with advanced hepatocellular carcinoma. Biomark Res 2024;12:26.
[9] Llovet JM, Castet F, Heikenwalder M, et al. Immunotherapies for hepatocellular carcinoma. Nat Rev Clin Oncol 2022;19:151–172.
[10] **Zhu AX**, **Abbas AR**, **de Galarreta MR**, et al. Molecular correlates of clinical response and resistance to atezolizumab in combination with bevacizumab in advanced hepatocellular carcinoma. Nat Med 2022;28:1599–1611.
[11] Sangro B, Sarobe P, Hervas-Stubbs S, Melero I. Advances in immunotherapy for hepatocellular carcinoma. Nat Rev Gastroenterol Hepatol 2021;18:525–543.
[12] **Ozeki Y**, **Kanogawa N**, Ogasawara S, et al. Liver biopsy technique in the era of genomic cancer therapies: a single-center retrospective analysis. Int J Clin Oncol 2022;27:1459–1466.
[13] Brackenier C, Kinget L, Cappuyns S, et al. Unraveling the synergy between atezolizumab and bevacizumab for the treatment of hepatocellular carcinoma. Cancers (Basel) 2023;15:348.
[14] **Kumagai S**, **Togashi Y**, **Kamada T**, et al. The PD-1 expression balance between effector and regulatory T cells predicts the clinical efficacy of PD-1 blockade therapies. Nat Immunol 2020;21:1346–1358.
[15] Denize T, Jegede OA, Matar S, et al. PD-1 Expression on intratumoral regulatory T cells is associated with lack of benefit from anti-PD-1 therapy in metastatic clear cell renal cell carcinoma patients. Clin Cancer Res 2024;30:803–813.
[16] Hoshida Y, Nijman SM, Kobayashi M, et al. Integrative transcriptome analysis reveals common molecular subclasses of human hepatocellular carcinoma. Cancer Res 2009;69:7385–7392.
[17] **Montironi C**, **Castet F**, **Haber PK**, et al. Inflamed and non-inflamed classes of HCC: a revised immunogenomic classification. Gut 2023;72:129–140.
[18] Sangro B, Melero I, Wadhawan S, et al. Association of inflammatory biomarkers with clinical outcomes in nivolumab-treated patients with advanced hepatocellular carcinoma. J Hepatol 2020;73:1460–1469.
[19] Haber PK, Castet F, Torres-Martin M, et al. Molecular markers of response to anti-PD1 therapy in advanced hepatocellular carcinoma. Gastroenterology 2023;164:72–88.e18.
[20] Yoshihara K, Shahmoradgoli M, Martinez E, et al. Inferring tumour purity and stromal and immune cell admixture from expression data. Nat Commun 2013;4:2612.
[21] Rooney MS, Shukla SA, Wu CJ, et al. Molecular and genetic properties of tumors associated with local immune cytolytic activity. Cell 2015;160:48–61.
[22] Ayers M, Lunceford J, Nebozhyn M, et al. IFN-gamma-related mRNA profile predicts clinical response to PD-1 blockade. J Clin Invest 2017;127:2930–2940.
[23] Kurebayashi Y, Matsuda K, Ueno A, et al. Immunovascular classification of HCC reflects reciprocal interaction between immune and angiogenic tumor microenvironments. Hepatology 2022;75:1139–1153.
[24] Sia D, Jiao Y, Martinez-Quetglas I, et al. Identification of an immune-specific class of hepatocellular carcinoma, based on molecular features. Gastroenterology 2017;153:812–826.
[25] Cappuyns S, Philips G, Vandecaveye V, et al. PD-1(-) CD45RA(+) effector-memory CD8 T cells and CXCL10(+) macrophages are associated with response to atezolizumab plus bevacizumab in advanced hepatocellular carcinoma. Nat Commun 2023;14:7825.
[26] **Magen A**, **Hamon P**, Fiaschi N, et al. Intratumoral dendritic cell-CD4(+) T helper cell niches enable CD8(+) T cell differentiation following PD-1 blockade in hepatocellular carcinoma. Nat Med 2023;29:1389–1399.
[27] Desert R, Chen W, Ge X, et al. Hepatocellular carcinomas, exhibiting intratumor fibrosis, express cancer-specific extracellular matrix remodeling and WNT/TGFB signatures, associated with poor outcome. Hepatology 2023;78:741–757.
[28] Greten TF, Sangro B. Targets for immunotherapy of liver cancer. J Hepatol 2018;68:157–166.
[29] Kamada T, Togashi Y, Tay C, et al. PD-1(+) regulatory T cells amplified by PD-1 blockade promote hyperprogression of cancer. Proc Natl Acad Sci U S A 2019;116:9999–10008.
[30] Nakagawa M, Inoue M, Ogasawara S, et al. Clinical effects and emerging issues of atezolizumab plus bevacizumab in patients with advanced hepatocellular carcinoma from Japanese real-world practice. Cancer 2023;129:590–599.
[31] Datta M, Coussens LM, Nishikawa H, et al. Reprogramming the tumor microenvironment to improve immunotherapy: emerging strategies and combination therapies. Am Soc Clin Oncol Educ Book 2019;39:165–174.
[32] Kurebayashi Y, Sugimoto K, Tsujikawa H, et al. Spatial dynamics of T- and B-cell responses predicts clinical outcome of resectable and unresectable hepatocellular carcinoma. Clin Cancer Res 2024;30:5666–5680.
[33] Sahai E, Astsaturov I, Cukierman E, et al. A framework for advancing our understanding of cancer-associated fibroblasts. Nat Rev Cancer 2020;20:174–186.

[34] Curti BD, Koguchi Y, Leidner RS, et al. Enhancing clinical and immunological effects of anti-PD-1 with belapectin, a galectin-3 inhibitor. J Immunother Cancer 2021;9:e002371.
[35] Henderson NC, Mackinnon AC, Farnworth SL, et al. Galectin-3 regulates myofibroblast activation and hepatic fibrosis. Proc Natl Acad Sci U S A 2006;103:5060–5065.
[36] Chalasani N, Abdelmalek MF, Garcia-Tsao G, et al. Effects of belapectin, an inhibitor of galectin-3, in patients with nonalcoholic steatohepatitis with cirrhosis and portal hypertension. Gastroenterology 2020;158:1334. 45.e5.
[37] Farhad M, Rolig AS, Redmond WL. The role of galectin-3 in modulating tumor growth and immunosuppression within the tumor microenvironment. Oncoimmunology 2018;7:e1434467.
[38] Peng X, Gong C, Zhang W, Zhou A. Advanced development of biomarkers for immunotherapy in hepatocellular carcinoma. Front Oncol 2022;12:1091088.
[39] Ercan C, Renne SL, Di Tommaso L, et al. Hepatocellular carcinoma immune microenvironment analysis: a comprehensive assessment with computational and classical pathology. Clin Cancer Res 2024;30:5105–5115.
[40] Myojin Y, Babaei S, Trehan R, et al. Multiomics analysis of immune correlatives in hepatocellular carcinoma patients treated with tremelimumab plus durvalumab. Gut 2025;74:983–995.
[41] Fukumura D, Kloepper J, Amoozgar Z, et al. Enhancing cancer immunotherapy using antiangiogenics: opportunities and challenges. Nat Rev Clin Oncol 2018;15:325–340.

Keywords: atezolizumab; bevacizumab; immunotherapy; hepatocellular carcinoma; tumor-infiltrating lymphocyte; tumor microenvironment.

Received 26 April 2025; received in revised form 22 September 2025; accepted 25 September 2025; Available online 1 October 2025